JMEPEG (2008) 17:651–661
DOI: 10.1007/s11665-007-9197-x

1059-9495/$19.00

Inverse Analysis of Heat Conduction in Hollow Cylinders with Asymmetric Source Distributions

Samuel G. Lambrakos, John G. Michopoulos, Harry N. Jones, and Craig N. Boyer

(Submitted November 13, 2007; in revised form December 4, 2007)

This paper presents an application of inverse analysis for determining both the temperature field histories and corresponding heat source distributions in hollow cylinders. The primary goal, however, is the development of an inversion infrastructure in a manner that allows taking advantage of all aspects related to its utility, including sensitivity analysis. The conditions generating heat sources are those resulting from intense pulsed-current electrical contact experiments. Under these conditions intense heat currents are generated due to the Joule conversion of the electric conduction currents. Asymmetry of the heat source is induced from the localized melting due to arc-enhanced electric conduction. Experimentally acquired temperature histories and melting domain boundary data are utilized to setup an inverse model of the heat conduction problem. This permits the construction of an estimate not only of the temperature field histories throughout the computational domain but also of an evaluation of the effective thermal diffusivity of the material involved.

Keywords advanced characterization, modeling processes, non-destructive testing

1. Introduction

During relatively intense pulsed-current (~35 kA peak) electrical conduction experiments of hollow cylinders in contact, under static mechanical load, both electric and heat current fluxes dominate the behavior of the associated contact surfaces (Ref 1). Under certain conditions post mortem melting profiles on the contact metal surface suggest the emergence of asymmetric temperature fields that can be modeled via the consideration of corresponding asymmetric heat source distributions. Because these types of contact experiments are necessary to help the understanding of the phenomena involved, it is important that one is able to invert real-time and post mortem data to establish insight into the nature of the heat and electric conduction involved. The overall context of this effort concerns investigation of metal-to-metal high-current contacts as a function of materials and pressure with potential applications to the arcing contacts involved in electromagnetic launch systems.

A data driven inverse analysis of unsteady heat conduction within hollow cylindrical structures is presented where the conduction is asymmetric relative to the cylindrical axis because of asymmetric source distributions. A significant aspect of this inverse analysis is that it is based on a model representation having a relatively small number of adjustable parameters. Methods of inverse analysis, in contrast to analysis methods based on the direct-problem approach, are characterized by many properties that follow directly from the fact that inverse methods are data driven as well as model driven (Ref 2, 3). Principal among these properties is the fact that relatively complex and highly nonlinear systems can be represented accurately by means of model representations characterized by small numbers of parameters. In many cases the errors that are introduced by approximations underlying an inverse model, and its associated relatively small number of parameters, are in fact compensated for by the characteristics of the data space.

A statement of the specific inverse problem to be considered is given, followed by a derivation of an inverse model for analysis of asymmetric and unsteady heat conduction within cylindrical structures that is characterized by a small number of parameters. Accordingly, a small number of model parameters provides for convenient and practical optimization of parameter values relative to a given data space consisting of measured temperature values or observations of phase transformations, e.g., solidification. The primary goal of this paper, however, is the development of an inversion infrastructure in a manner that provides advantages relative to all aspects related to its utility, including sensitivity analysis.

The physical assumptions and mathematical approximations underlying this derivation are elucidated. A discussion is then presented of specific aspects of the inverse model within the context and objectives of the general inverse heat transfer problem. Subsequently, the inverse model is applied to the analysis of heat conduction within a metal cylinder resulting from localized heating due to pulsed currents through the cylinder. Discussion of the results of this analysis considers their significance relative to multiscale modeling of heat conduction in cylinders. In particular, what characteristics of the heat source can be reconstructed from inverse analysis using the model, and accordingly, what characteristics of the calculated temperature field are to be adopted and are well posed for multiscale modeling. Subsequently, the analysis is

Samuel G. Lambrakos, John G. Michopoulos, and **Harry N. Jones**, Material Sciences Division, Naval Research Laboratory, Washington, DC; and **Craig N. Boyer**, Titan Corporation, Reston, VA. Contact e-mail: sam.lambrakos@nrl.navy.mil.

extended to consider sensitivity to the influence of changes in the spatial distribution of the heat source as governed by the current pulse. For this sensitivity analysis we have adopted a heat source distribution whose general shape is more closely correlated with the experimentally observed shape of the melted region of the cylinder. The final section of the presentation considers multiscale methodologies for coupling results from inverse analysis to models that are characterized by relatively more detailed physical representations of energy sources.

2. Statement of Inverse Problem

The inverse problem concerning analysis of physical processes, in general (Ref 4), and the inverse heat transfer problem, in particular (Ref 5), may be stated formally in terms of source functions (or input quantities) and multidimensional fields (output quantities). Other investigators have also focused on various aspects of inverse problems related to heat deposition processes especially as they relate to the determination of heat fluxes via appropriate regularization of their spatial and time distributions (Ref 6). In general, the formulation of a heat conductive system occupying an open bounded domain Ω with an outer boundary Γ_o and an inner boundary Γ_i involves the parabolic equation

$$\frac{\partial T(\mathbf{x},t)}{\partial t} = \nabla \cdot (\kappa(\mathbf{x},t)\nabla T(\mathbf{x},t)) \text{ in } \Omega \times (0,t_f), \qquad \text{(Eq 1a)}$$

with initial condition

$$T(\mathbf{x},0) = T_0(\mathbf{x}) \text{ in } \Omega, \qquad \text{(Eq 1b)}$$

and heat flux exchanges through the outer and inner boundaries Γ_o and Γ_i as follows:

$$-\kappa(\mathbf{x},t)\frac{\partial T(\mathbf{x},t)}{\partial n_{\Gamma_o}} = c(\mathbf{x},t)(T(\mathbf{x},t) - T_a(\mathbf{x},t)) \text{ on } \Gamma_0 \times (0,t_f), \qquad \text{(Eq 1c)}$$

$$-\kappa(\mathbf{x},t)\frac{\partial T(\mathbf{x},t)}{\partial n_{\Gamma_i}} = q(\mathbf{x},t) \text{ on } \Gamma_i \times (0,t_f). \qquad \text{(Eq 1d)}$$

Here $\mathbf{x} = (x,y,z)$ is the position vector; n_{Γ_o} and n_{Γ_i} are the normal vectors onto boundaries Γ_o and Γ_i, respectively; t is the time variable; t_f is the final time; $T(\mathbf{x},t) = T(x,y,z,t)$ is the temperature field variable; $\kappa(\mathbf{x},t) = \kappa(x,y,z,t)$ is the heat conductivity field variable (i.e., diffusivity); $c(\mathbf{x},t) = c(x,y,z,t)$ and $T_a(\mathbf{x},t) = T_a(x,y,z,t)$ are specified functions; and $q(\mathbf{x},t) = q(x,y,z,t)$ is the heat flux on the inner boundary Γ_i. Determination of the temperature field via the solution of Eq 1(a) to (d) constitutes the so-called forward or direct initial-boundary value problem. Our interest here, however, is focused on that of a formulation outlining the inverse problem and can be stated as follows: Effectively reconstruct the heat flux field $q(x,y,z,t)$ on the inner boundary Γ_i, and the resulting temperature field $T(x,y,z,t)$ for all time $t \in [0,t_f]$ when the boundary Γ_i is totally or partially inaccessible. To reconstruct the heat flux, additional information concerning the temperature $T(x,y,z,t)$ is needed (i.e., known values that have been acquired experimentally) (Ref 4, 6).

In the present analysis the inverse problem is defined in the context of the two cylinders in contact as shown in Fig. 1. According to Fig. 1, it is noted that the source function

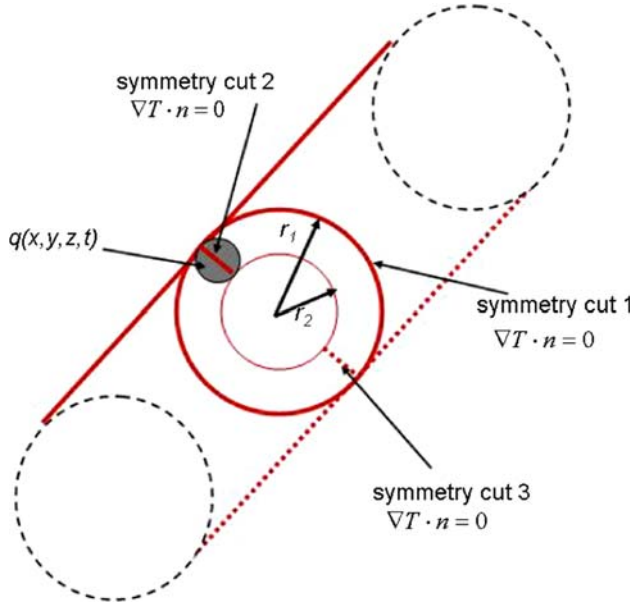

Fig. 1 Hollow cylinder domain defining inverse heat transfer problem

$q(x,y,z,t)$ is to be determined in terms of its volumetric spatial and temporal characteristics.

Further, additional information that is needed lies within a data space for analysis of this system that in general consists of (a) measurements of the temperature $T(x,y,z,t)$ at different locations and times on the surface of the cylinder, e.g., thermocouple measurements, (b) the location of the central point of the source function $q(x,y,z,t)$ within the volume of the hollow cylindrical structure, e.g., post mortem melting profiles on the contact metal surface, (c) information concerning the spatial and temporal characteristics of the source function $q(x,y,z,t)$, and (d) information concerning the thermal diffusivity of the material.

Information concerning the spatial and temporal characteristics of $q(x,y,z,t)$ would in principle include the shapes of solidification boundaries resulting from localized melting. Information concerning the thermal diffusivity of the material would be the average diffusivity for a range of temperatures.

Our derivation of a minimal parameterization for representation of asymmetric and unsteady heat conduction within cylindrical structures follows from the construction of a one-to-one mapping from the geometry of a cylindrical structure into that of a bounded plate structure. Referring to Fig. 2, it can be observed that the presence of an asymmetrically located energy source within the volume of the cylinder actually introduces physical conditions that permit, mathematically, the introduction of a symmetry cut within the cylindrical structure that intersects the central point of the source function $q(x,y,z,t)$. This symmetry cut, i.e., symmetry cut 2 in Fig. 1, permits a mapping of the cylindrical domain, having one asymmetrically located source, into a planar domain of finite thickness, having two energy sources of equal strength that are located symmetrically on the boundaries of the domain. A condition for the accuracy of this mapping is that the aspect ratio, defined by the quantity

$$\delta = (r_1 - r_2)/r_2, \qquad \text{(Eq 2)}$$

be sufficiently small relative to dominant spatial shape features of the source function $q(x,y,z,t)$. For unsteady heat deposition within a planar structure of finite thickness a consistent

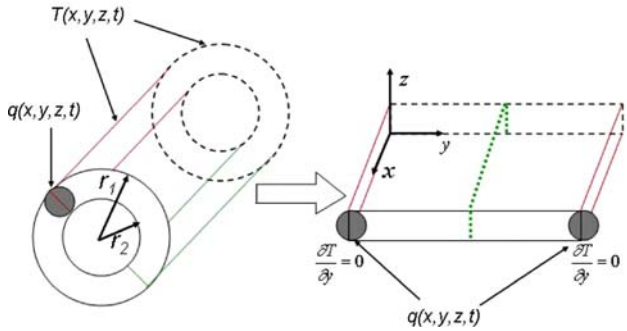

Fig. 2 Hollow cylinder domain after the cut-1 (left) and its transformation to simple rectangular domain after cut-2 (right)

parametric representation of the time-dependent temperature field is constructed from basis functions satisfying Eq 1(a) according to

$$T(x,y,z,t) = T_A + \sum_{k=1}^{N_k}\sum_{n=1}^{N_t} T_k(\hat{x},\hat{x}_k,n\Delta t), \qquad \text{(Eq 3a)}$$

where

$$T_k(\hat{x},\hat{x}_k,n\Delta t) = \frac{C(x_k,y_k,z_k)}{(n\Delta t)}\exp\left[-\frac{(x-x_k)^2+(y-y_k)^2}{4\kappa(n\Delta t)}\right] \times\left\{1+2\sum_{m=1}^{\infty}\exp\left[-\frac{\kappa m^2\pi^2(n\Delta t)}{l^2}\right]\cos\left[\frac{m\pi z}{l}\right]\cos\left[\frac{m\pi z_k}{l}\right]\right\}, \qquad \text{(Eq 3b)}$$

The quantity l is the thickness of the planar structure, which for the mapping defined by Fig. 2 is equal to $(r_1 - r_2)$. The vectors $\hat{x} = (x,y,z)$ are positions within the structure and $\hat{x}_k = (x_k,y_k,z_k)$, $k = 1,\ldots,N_k$ are the locations of the elemental heat sources. The quantities Δt and n are the timestep and timestep index, respectively, where the time $t = n\Delta t$.

3. Prototype Measurements

Presented in this section is a description of the experimental measurements adopted for inverse analysis. Details concerning the experimental arrangement and procedure used for these measurements are given in reference (Ref 1). The experimental arrangement consists of a load frame equipped with an electrically insulated load train to establish a contact force on a metal-metal interface through which a pulsed current is transmitted. The time-dependent evolution of the voltage drop across the interface is recorded during a 40-kA peak current pulse having a 300-μs rise time with peak current densities of the order of 39 kA/cm^2. The interface stack was assembled from two pieces of 4130 steel each having a 12-mm outside diameter with a 6.3-mm hole (see Fig. 3 and 4). It should be noted that Fig. 3 and 4 correspond to different experiments.

Heat transfer within the cylinder resulting from the current pulse is monitored using thermocouple measurements and correlation of local heating with the post mortem melting profile on the contact metal surface. Thermocouples were fabricated from Type K 5 mil wire. These were spot welded to the 4130 steel using this same material as an intermediate metal to

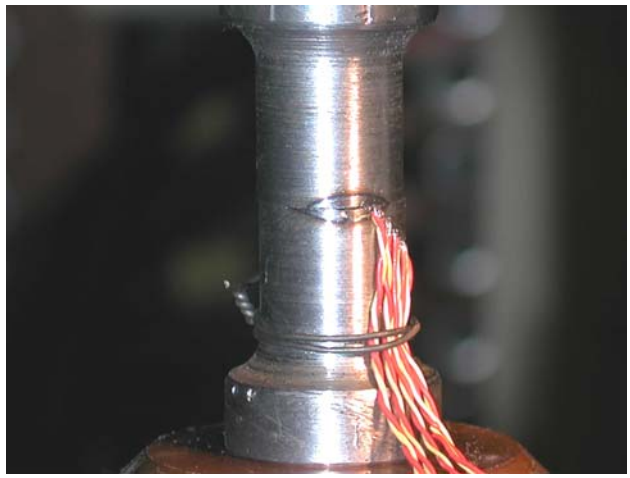

Fig. 3 Melt profile on side surface of 4130 steel cylinder

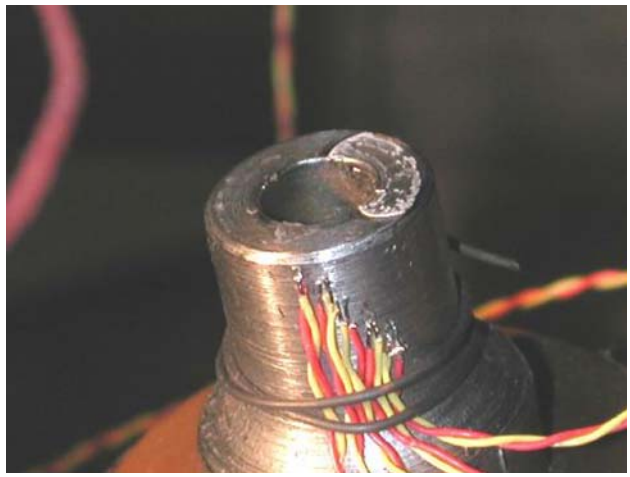

Fig. 4 Melt profile on contact surface and relative locations of thermocouple attachments

minimize thermocouple lag and intrinsic error. The thermocouple amplifiers (5B modules) were chopper isolated with a 4-Hz low pass filter. As a consequence of this signal filtering valid temperatures are not measured until a settling time of around 250 ms after the pulse is initiated. Since the total duration of the current pulse is 13 ms all valid temperature measurements are made with no currents imposing stray voltages on the thermocouples. The present data-driven inverse analysis considers parameter optimization with respect to the data set consisting of the melting profile at the surface (Fig. 4), measurements of temperature histories at locations on the cylinder (see Fig. 5), the characteristics of the pulsed current (Fig. 6), and the average material and thermal properties of 4130 steel. These average properties are a density ρ = 7.84 g/cm^3, thermal conductivity k = 42.7 W/m-K, specific heat C_p = 477 J/kg-K, and the melting temperature T_M = 1432 °C.

4. Inverse Analysis

As mentioned earlier, inverse heat transfer analysis deals with the problem of identifying the heat source distribution and

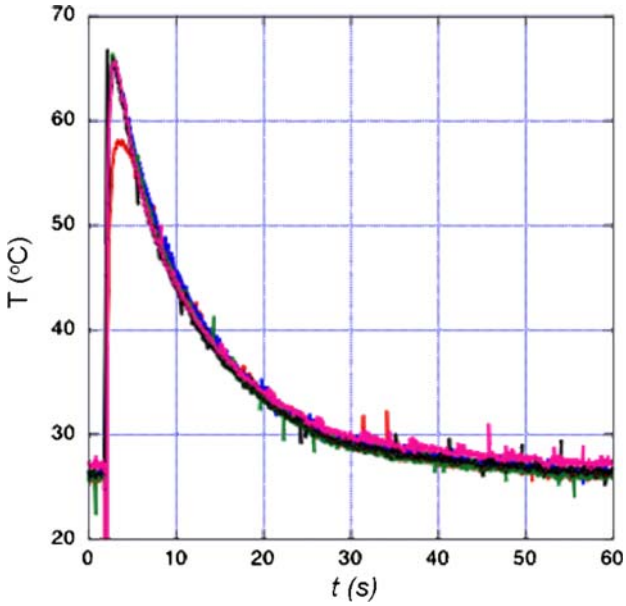

Fig. 5 Temperature histories measured using thermocouples

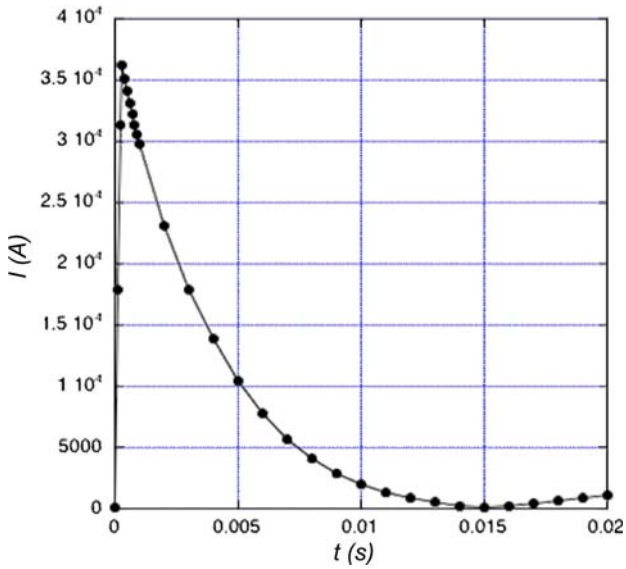

Fig. 6 Pulsed current characteristics for the thermal effect experiments

the associated temperature field everywhere within a region of interest, based on partial data available in that region as well as in the region of the heat source. When the temperature field is known directly through sensor data (e.g., thermocouple measurements) or indirectly (e.g., through phase transformation boundaries) at specific points within the region of interest, constraint conditions of form

$$T(x_{\mathrm{m}}^{\mathrm{c}}, y_{\mathrm{m}}^{\mathrm{c}}, z_{\mathrm{m}}^{\mathrm{c}}, t_{\mathrm{m}}^{\mathrm{c}}) = T_{\mathrm{m}}^{\mathrm{C}}, \qquad \text{(Eq 4)}$$

must be satisfied by the parametric representation adopted for the temperature field, i.e., the functions $T_k(x,y,z,t)$ of Eq 3. In general, the only requirement for the functions $T_k(x,y,z,t)$ making up the linear combination defined by Eq 3 is that they have trends consistent with that of the temperature field associated with the specific heat deposition process.

It is important to mention here that the reconstruction of the heat flux distribution problem is known to be severely ill-posed (Ref 4, 6). One of the main difficulties associated with the field reconstruction comes from both the space and time dependence of the heat flux and the fact that the inner boundary defined by symmetry cuts 1 and 2 is relatively far from the region where measurements are made. The most severe instability of an inverse problem is triggered when the reconstruction involves determination of the field profile at the initial time and over a large boundary of the physical domain (Ref 6). Various investigators have introduced regularization methodologies to deal with this problem (Ref 6-10). In our case, as indicated from the experimental setup, the heat flux region is nucleating from a highly localized region that is not far from the region where measurements are performed.

The formal procedure underlying the inverse method considered here entails the adjustment of a representation for the temperature field $T(x,y,z,t)$ defined over the entire spatial region of the system of interest. This approach defines an optimization procedure where a temperature field spanning the spatial region of the system of interest is adopted as the quantity to be identified. Accordingly, an optimization criterion may be defined by minimizing the value of an objective function of the form

$$Z = \sum_{m=1}^{N_m} w_{\mathrm{m}} \left(T(x_{\mathrm{m}}^{\mathrm{c}}, y_{\mathrm{m}}^{\mathrm{c}}, z_{\mathrm{m}}^{\mathrm{c}}, t_{\mathrm{m}}^{\mathrm{c}}) - T_{\mathrm{m}}^{\mathrm{C}} \right)^2, \qquad \text{(Eq 5)}$$

where w_{m} are weight coefficients and the quantities with superscript "c" designate constraints on temperatures or positions within the structure at specific times. The mathematical structure underlying the general formulation defined by Eq 3 through Eq 5 is that of a parametric function-approximation that employs a linear combination of nonlinear functions. This structure establishes equivalence between inverse methods and methods of constrained parameter optimization. The mathematical structure of the formulation defined by Eq 3 through Eq 5 provides for the inclusion of information either through specification of constraints $T_{\mathrm{m}}^{\mathrm{C}}$ or the functions $T_k(x,y,z,t)$.

Throughout the development that follows consideration is given to different spatial and temporal regimes of the temperature field. Each of these regimes is characterized by a characteristic length and time scale. In that the development is a framework for inverse analysis, consideration tends to be given initially to temperature field regimes associated with spatial locations that are relatively remote from the energy source (thermocouple measurements) or times that are long relative to the characteristic duration time of energy input to the system. Accordingly, subsequent analysis considers regions of the temperature field that are associated with successively smaller characteristic length and time scales.

5. Specification of Adjustable Parameters

The quantities $C(x_k,y_k,z_k)$, $k = 1,\ldots,N_k$, define a discrete distribution of elemental heat sources. The present analysis considers detailed information concerning the spatial distribution of heat that is coupled into the system. Accordingly, this analysis considers correlation of the calculated solid-liquid interface as discussed below with that which is experimentally

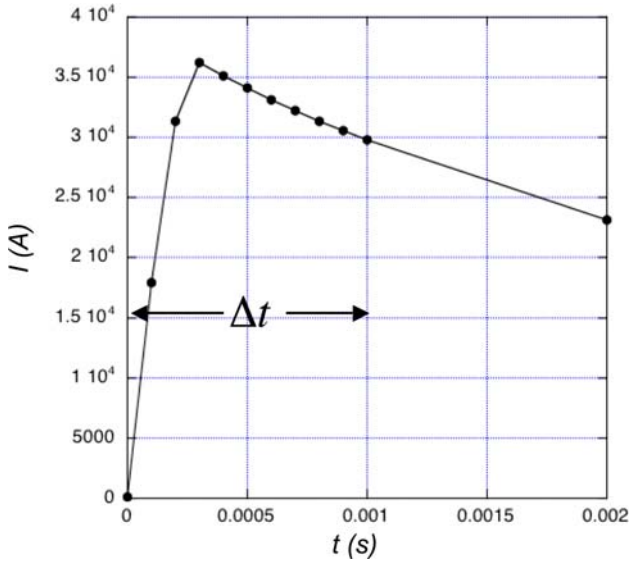

Fig. 7 Comparison of timestep to onset of current pulse

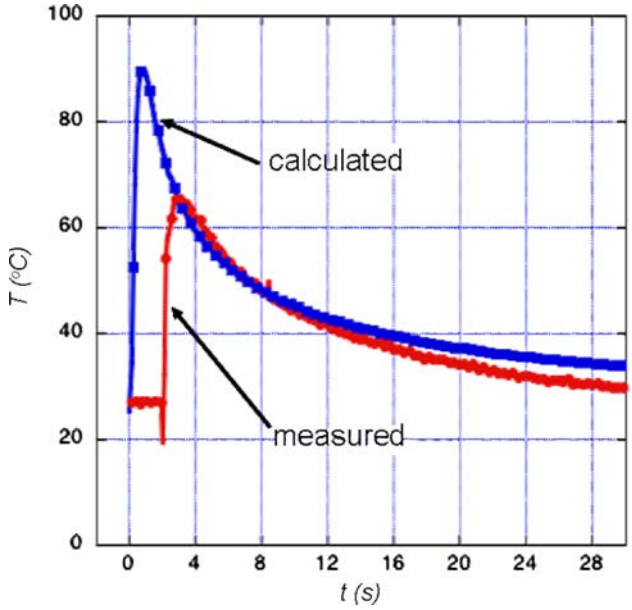

Fig. 8 Calculated temperature field based on minimization of objective function with respect to adjustment of parameters $C(x_1,y_1,z_1)$, Δt and κ

observed (see Fig. 4 above). In addition, this analysis considers the sensitivity of the calculated temperature field with respect to the shape of the heat source distribution. Accordingly, two distinctly different heat source distributions are adopted for analysis. These are a point source distribution, i.e., the single term $k = 1$ in Eq 3 and a line source distribution, i.e., $C(x_o,y_k,z_o)$, $k = 1,\ldots,N_k$, in Eq 3, where the values of x_o and z_o are fixed. The initial analysis considers the set of model parameters consisting of the quantities $C(x_1,y_1,z_1)$, Δt and κ. The timestep Δt is assigned a value of 0.001 s based on the measured rise time of the current pulse (see Fig. 7) and sufficient correlation between observed and calculated near-source temperature field values. Accordingly, for the initial analysis objective function minimization is with respect to the three adjustable parameters $C(x_1,y_1,z_1)$, Δt, and κ. The diffusivity κ is assigned an initial estimate of 1.142×10^{-5} m^2/s based on the average thermal properties of 4130 steel. In general, determination of a multistage thermal diffusivity requires that the objective function Eq 5 be minimized relative to temperature field values that span both far-field and near-source regions of the temperature field. This type of minimization, which is with respect to different temperature and time scales, requires a sufficient number of adjustable parameters such that the system is not underspecified. The present analysis considers initially a minimal parameter set consisting of three parameters, $C(x_1,y_1,z_1)$, Δt, and κ. Subsequent analyses consider parameter sets consisting of four parameters, $C(x_o,y_k,z_o)$, N_k, Δt, and κ, and of five parameters, $C(x_o,y_k,z_o)$, N_k, Δt, κ, τ_1, and τ_2, where τ_1 and τ_2 are time shift and time delay parameters, respectively.

6. Parameter Estimation

For the data space considered in this analysis, consisting of the melting profile at the surface (Fig. 4), measurements of temperature histories at locations on the cylinder (see Fig. 5), the characteristics of the pulsed current (Fig. 6), and thermal properties of 4130 steel, a relatively optimal and minimal set of parameter values is given by ($C(x_1,y_1,z_1)$, Δt, κ) = (31.0 °C-s, 0.001 s, 2.5×10^{-5} m^2/s). The correlation between calculated and experimentally observed field values is examined with reference to Fig. 8-13, which span both far-field and near-source regions of the temperature field. Correlation with far-field regions of the temperature field is shown by Fig. 8. Referring to this figure, one observes good correlation for temperature values above 40 °C. In principle, one would expect a deviation at lower temperatures in that the calculated value of κ is weighted relative to a range of temperatures and thermal diffusivity is actually a function of temperature whose value tends to increase with temperature for metals. In addition, it is significant to note that near-source regions of the temperature field may not be in a state of thermodynamic equilibrium at times during the initiation of energy input to the system, i.e., the period of time shown in Fig. 6.

Shown in Fig. 9 is the evolution of the temperature field at times where the spatial distribution of heat tends toward homogeneity. Physically this corresponds approximately to the time period where the wavefronts of the two identical heat waves generated by the source meet at symmetry cut 3 shown in Fig. 1. The far-field and long-time trends of the temperature field are certainly important for inverse analysis in that these trends establish constraints on the near-source regions and energy-input period. The essentially asymptotic region of the temperature field, however, is characterized by a lack of structure (see Fig. 9), and therefore, any parameterization of this region does not provide information related to near-source or short time scale trends. In contrast, temporal characteristics of the temperature field, during passage of the heat wave generated by the source, at spatial locations that are close to it, are relatively rich in terms of structure. Therefore, this temporal region contains information concerning the characteristics of the near-source and short time scale trends of the temperature field. Parameter optimization with respect to near-source regions of the temperature field requires simulation of the heat

wavefront at the location of the thermocouple that is consistent with the energy source characteristics and near-source temperature field values. Shown in Fig. 10 are the temporal characteristics of the calculated heat wave at the position of the thermocouple whose measurements have been adopted as constraint conditions. Referring to this figure, it is to be noted that the time for passage of the wavefront is approximately 1 s.

Shown in Fig. 11 are temperature contours for the evolution of the calculated temperature field within both near-source and far-field regions, following passage of the heat wavefront. The three domains shown in this figure have been separated at symmetry cuts 1, 2, and 3 defined in Fig. 1. Correlation of the near-source regions of the calculated temperature field with experimental measurements is demonstrated with reference to Fig. 11 and 12. In particular, shown in Fig. 12(a) and (b) is the time evolution of the solid-liquid interface occurring during the current pulse. It is significant to note that this calculated melt zone is sufficiently correlated with that which is experimentally observed (see Fig. 4) in that a point energy source was adopted for representation of the energy coupled into the system, rather than a spatial distribution of volumetrically deposited energy.

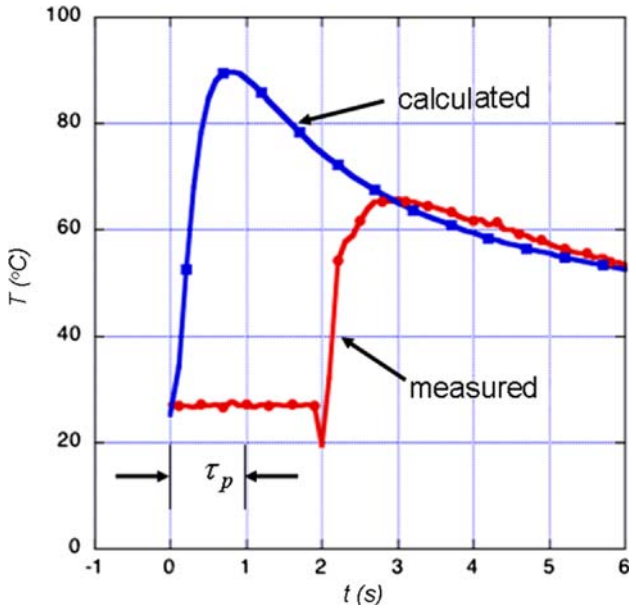

Fig. 9 Temperature field as times 8 and 14 s during onset of essentially equilibrated period of temperature history

A correlation of the calculated rate of energy deposition within the metal cylinder with experimentally observed characteristics of the pulsed current can be made as follows. Letting $Q(t)$ be the energy that has been coupled into the system at time t within a volume V_S, it follows that

$$Q(t) = \int_{x_1}^{x_2}\int_{y_1}^{y_2}\int_{z_1}^{z_2}\left[\int_{T_A}^{T(x,y,z,t)} \rho(T)C_p(T)dT\right]dxdydz, \qquad \text{(Eq 6)}$$

for energy deposition within a sample volume $V_S = (x_2 - x_1)(y_2 - y_1)(z_2 - z_1)$. It follows from the integral mean value theorem that

$$Q(t) = \langle \rho C_p \rangle V_S[T(x_1, y_1, z_1, t) - T_A]. \qquad \text{(Eq 7)}$$

Next, referring to Eq 3(a) and (b), it follows that

$$Q(t) \propto \frac{C(x_1, y_1, z_1)}{n\Delta t}. \qquad \text{(Eq 8)}$$

Next, it is to be noted that in principle

$$Q(t) = \eta IV, \qquad \text{(Eq 9)}$$

where η, I, and V are the coupling efficiency, current, and voltage, respectively, associated with the current pulse. Next, since $V = IR$, where R is the resistance, it follows that

$$Q(t) \propto I^2. \qquad \text{(Eq 10)}$$

Thus, correlation between the calculated and observed rate of energy deposition can be established by comparison of Eq 8 and 10. Shown in Fig. 13 are the rates of energy deposition calculated according to Eq 8 and 10, respectively. The values of Q and I^2, given in arbitrary units, have been scaled relative to the maximum value of I in Fig. 6. A comparison of the curves

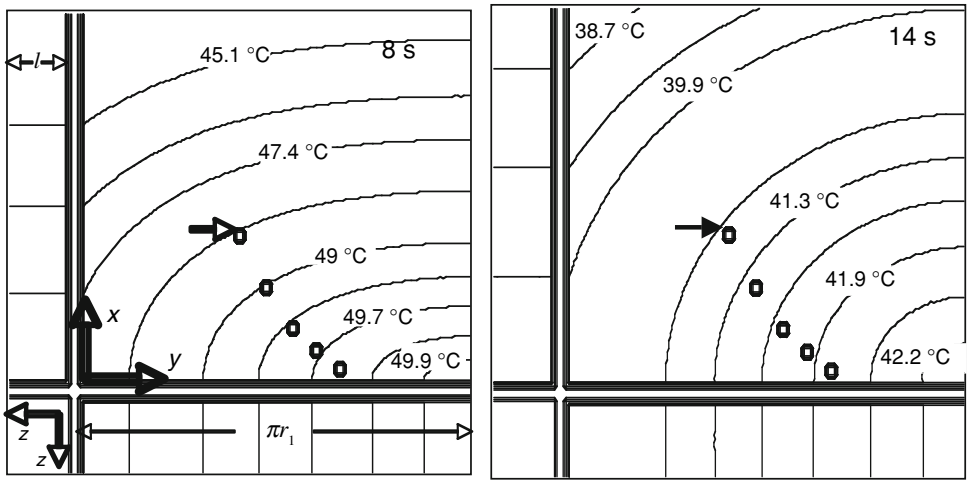

Fig. 10 Temperature history resulting from heat wave at location of thermocouple generated by current pulse where the time period for passage of the wavefront is approximately τ_p

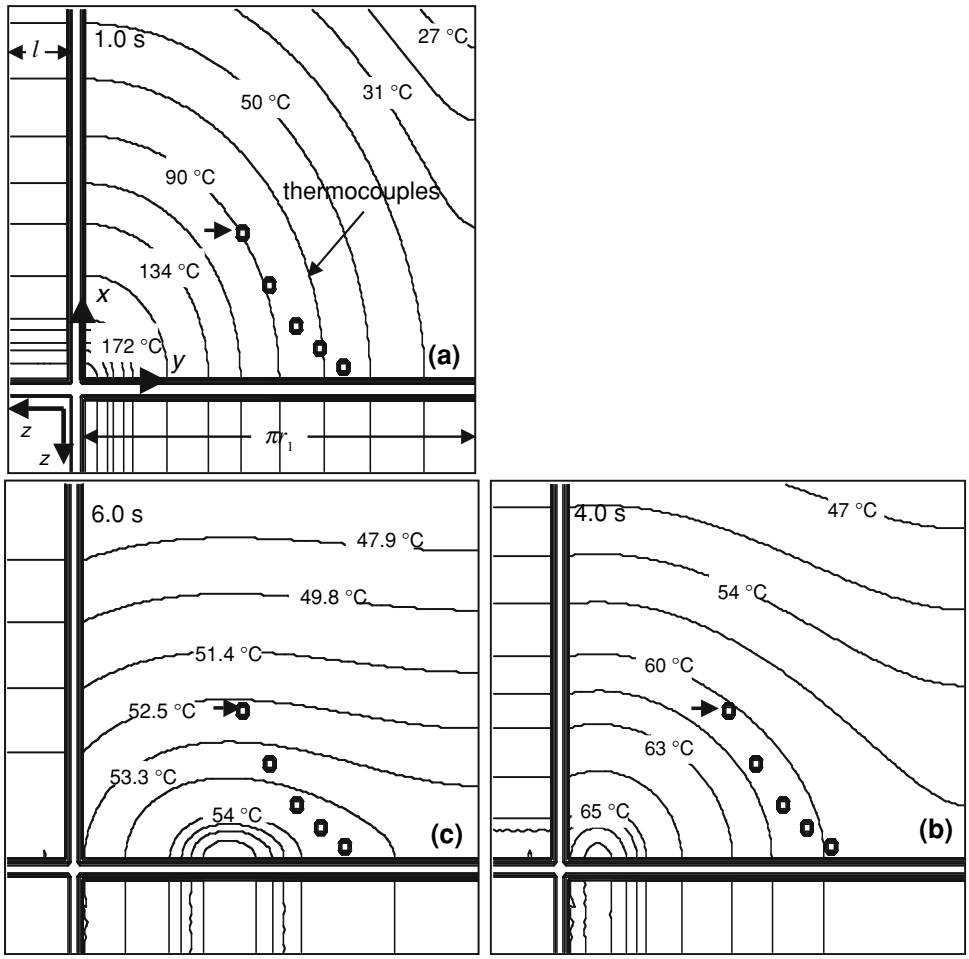

Fig. 11 Temperature field at times 1, 4, and 6 s following passage of heat wavefront at position of thermocouple indicated by arrow

shown in Fig. 13 indicates reasonable agreement between the two estimated rates of energy deposition.

7. Extension of Data and Parameter Sets

Referring to Fig. 12(a) to (d), it can be noted that spatial locations of the thermocouples are distributed such that there is identical sampling of the heat wave generated by the current pulse. This is in good agreement with the measured temperature histories shown in Fig. 5, which for different thermocouples are essentially the same. This suggests that a more optimal distribution of the thermocouple locations is such that at any given time different parts of the heat wave are sampled by each of the thermocouples. This type of spatial distribution of the thermocouple locations would also provide for the sampling of the heat wave within different temperature ranges and therefore generate a data set that is more multistage in character. Accordingly, the number of model parameters representing the system could be increased.

The thermal diffusivity κ is typically a function of temperature. The characteristic temperature dependence of κ for metals can be demonstrated with reference to Fig. 14. Referring to Fig. 14, it follows that representation of the thermal diffusivity κ can be extended by means of the parameterized functions of temperature

$$\kappa(T) = \sum_{i=0}^{2} a_{\mathrm{Si}} T^i \quad \text{(solid region)}, \qquad \text{(Eq 11)}$$

and

$$\kappa(T) = \sum_{i=0}^{2} a_{\mathrm{Li}} T^i \quad \text{(liquid region)}. \qquad \text{(Eq 12)}$$

It is significant to note, however, that the contributions due to the quadratic terms are typically very small. Therefore, the temperature dependence of the thermal diffusivity could in principle be represented by four parameters. In addition, the inherent nature of the temperature dependence of κ implies a step function response of the system to the transition from liquid to solid state. It follows that in general any parametric representation of the temperature field, within the solid region, can be effectively uncoupled from its trend characteristics within the liquid region. Accordingly, with respect to the temperature field spanning the solid region, the melted region assumes the role of an embedded boundary that can be characterized formally as an effective distributed source function.

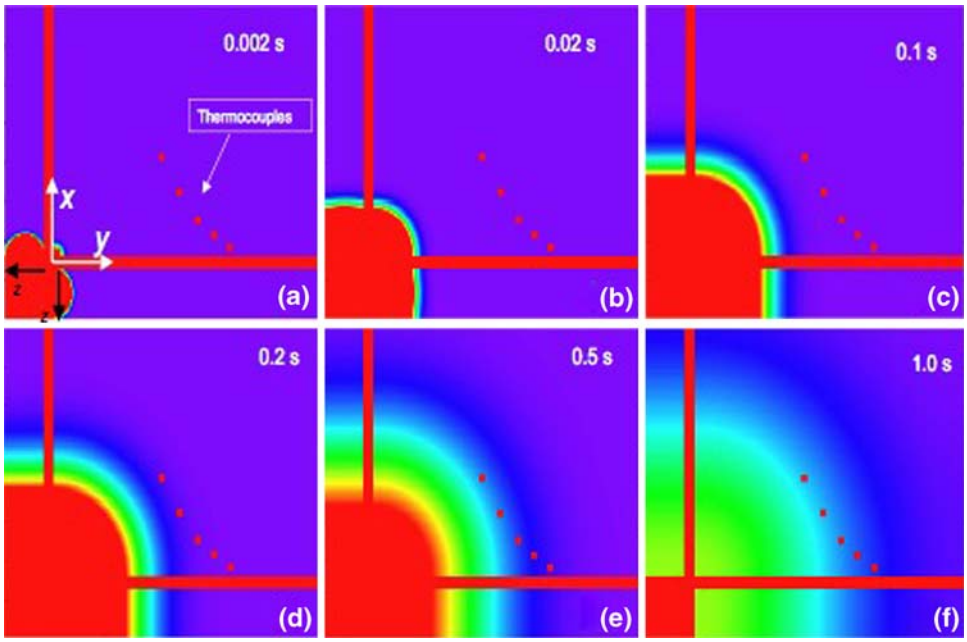

Fig. 12 Time evolution of solid-liquid interface during current pulse where point source distribution is assumed

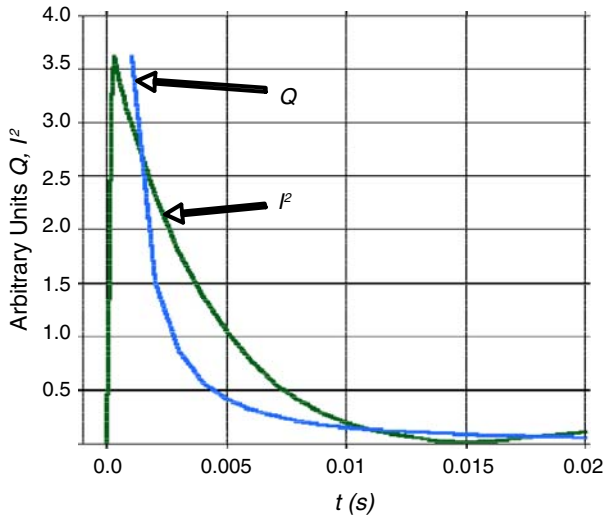

Fig. 13 Rates of energy deposition calculated according to Eq 8 and 10

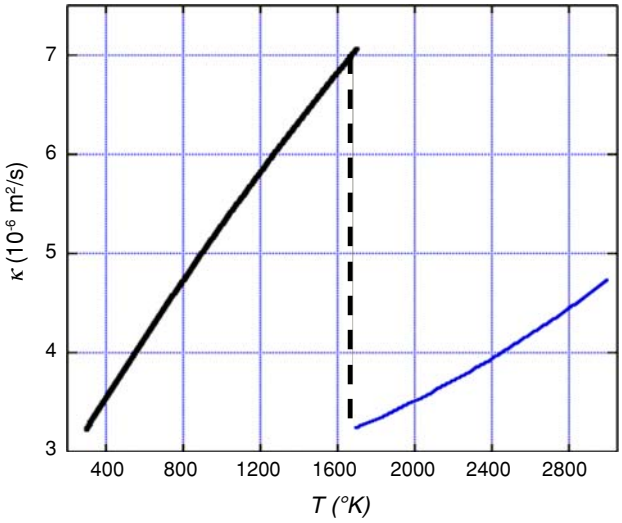

Fig. 14 Experimentally measured values of the thermal diffusivity of 304 stainless steel

Inclusion of detailed information concerning the shape of the melt region (e.g., Fig. 4) is achieved by parametric representation of the discrete distribution of elemental heat sources $C(x_k,y_k,z_k)$, $k = 1,\ldots,N_k$, defined in Eq 3. A physically plausible representation is given by

$$C(x_k,y_k,z_k) = C_0 \times \exp\left[-\alpha(x_k - x_0)^2 - \beta(y_k - y_0)^2 - \gamma(z_k - z_0)^2\right], \quad \text{(Eq 13)}$$

which would in principle introduce four additional parameters. At this stage it is significant to note that Eq 13 provides only a spatial representation of distribution of energy. This parameterization does not consider evolution of the volumetric distribution in time. It is therefore necessary to introduce additional adjustable parameters to represent the temporal, as well as spatial, characteristics of the energy deposit. Other temporal aspects of the system response that must be considered are the different types of possible time delays that could be associated with thermocouple measurements. This consideration is not restricted to the characteristic time delay associated with thermocouple response or the nature of thermocouple attachment. For the present analysis, we consider a parametric representation of time delay associated with thermocouple attachment that is due to the general experimental environment, which includes the influence of a current pulse. It follows that a consistent representation of thermocouple response requires at least two additional parameters. These would represent characteristic time delay associated with thermocouple measurement

and characteristic time shifts associated with the inherent temporal characteristics of the energy source. Accordingly, a consistent representation of these temporal characteristics is given by

$$T_{TC}(x,y,z,t) = [1 - \exp(-(t - \tau_1)/\tau_2)]T(x,y,z,t - \tau_1) \quad \text{(Eq 14)}$$

where T_{TC} and T are the measured and actual temperatures, respectively, τ_1 is the characteristic time shift associated with coupling of energy into the system, and τ_2 is the characteristic time delay of the thermocouple. It is significant to note that τ_1 is a minimal parametric representation of the step function response character of κ associated with the transition from liquid to solid state.

8. Sensitivity Analysis with Respect to Heat Source Distribution

In this section the analysis is extended to consider the influence of changes in the spatial distribution of heat that is coupled into the system by the current pulse. For this sensitivity analysis we have adopted a heat source distribution whose general shape is more closely correlated with the experimentally observed shape of the melted region of the cylinder (see Fig. 4). Accordingly, the line source or discrete uniform distribution,

$$C(x_1,y_k,z_1) = C_0; \quad k = 1,\ldots,N_k, \quad \text{(Eq 15)}$$

which provides a first approximation to Eq 13, is adopted for numerical simulation, where $C_0 = 7.75$ °C-s, $N_k = 20$, $(x_1,\ y_1,\ z_1) = (0.1425,\ 0.1425,\ 1.425$ mm) and $y_{k+1} - y_k = 0.1425$ mm.

It is significant to note that temporal changes of the heat source distribution occurring within the melted region are represented implicitly by the distribution of heat sources and can be quantified through specification of the temporal response parameters τ_1 and τ_2 defined with respect to Eq 14. Shown in Fig. 15 are the temperature histories of the measured and calculated heat waves, for both point and line heat source distributions, at the position of the thermocouple whose measurements have been adopted as constraint conditions. A comparison of the calculated temperature histories shows that the measured trend of the temperature field is relatively insensitive to spatial distribution of heat that is coupled into the system. This insensitivity is demonstrated by comparison of Fig. 12 and 16, which show the time evolution of the heat wavefront generated by point and line heat source distributions, respectively. In contrast, referring to Fig. 15, the region of the temperature history associated with the heat wavefront is relatively sensitive to spatial distribution of heat generated by the pulse. This result implies that a relatively detailed characterization of the melted region, as well as spatial and temporal trends associated with energy input to the system (e.g., Fig. 13), is important for the determination of peak temperatures within the near-source region of the system. The determination of peak temperatures is important in that these values can be correlated with solid-state transformations occurring within the material making up the system. Prediction of these solid-state transformations, quantitatively, can be correlated with system performance.

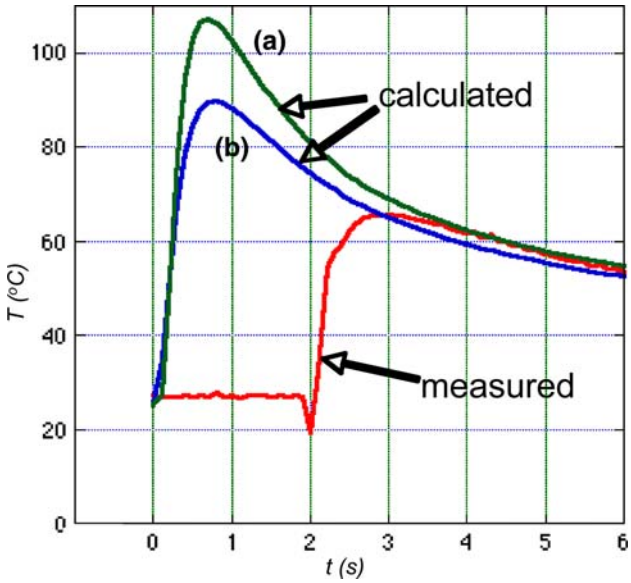

Fig. 15 Temperature history resulting from heat wave at location of thermocouple, where (a) and (b) are for point and line heat-source distributions, respectively

9. Parameterization of Temporal Response Characteristics

Temporal changes of the heat source distribution occurring within melted regions of the system are represented implicitly by the distribution of heat sources at a given instant of time, e.g., Eq 13 and 15. In particular, the heat source distribution can be interpreted as a generating function of the solidification boundary at a specific time. It also follows that the shape of the melted region is a function of the temperature dependence of the thermal diffusivity κ for temperatures above that of melting. These properties, together with the fact that the temperature dependence of κ implies a step function response of the system to the transition from liquid to solid state (see Fig. 14), provide a foundation for adopting τ_1 and τ_2 as process parameters for characterization of the system response (or in particular, material response) to pulse current at locations that are extremely local to the energy source. Accordingly, referring to Eq 14, the parameter τ_1 can represent the time required for evolution of the solidification boundary to that of a specified shape starting from the initiation of the current pulse. This process parameter can also be associated, in principle, with those characteristics of the system related to any time delay for energy input. The process parameter τ_2 represents the average cumulative delay in the measurement of temperature as a function of time due to external influences on the system and is not simply that of the characteristic time delay of thermocouples. Referring to Fig. 15, it should be noted that values of the parameters τ_1 and τ_2 can be determined by minimizing the difference between the calculated and measured temperature histories in the neighborhood of the maximum temperature according to Eq 14. Following this procedure for the case of the line heat-source distribution shown in Fig. 15, the measured and calculated temperature histories are related by Eq 14 for parameter values $(\tau_1,\ \tau_2) = (1$ s, 1.62 s). Whereas parameter τ_2 is to be related to any physical process influencing measurement of temperature as a function of time, the parameter τ_1 can

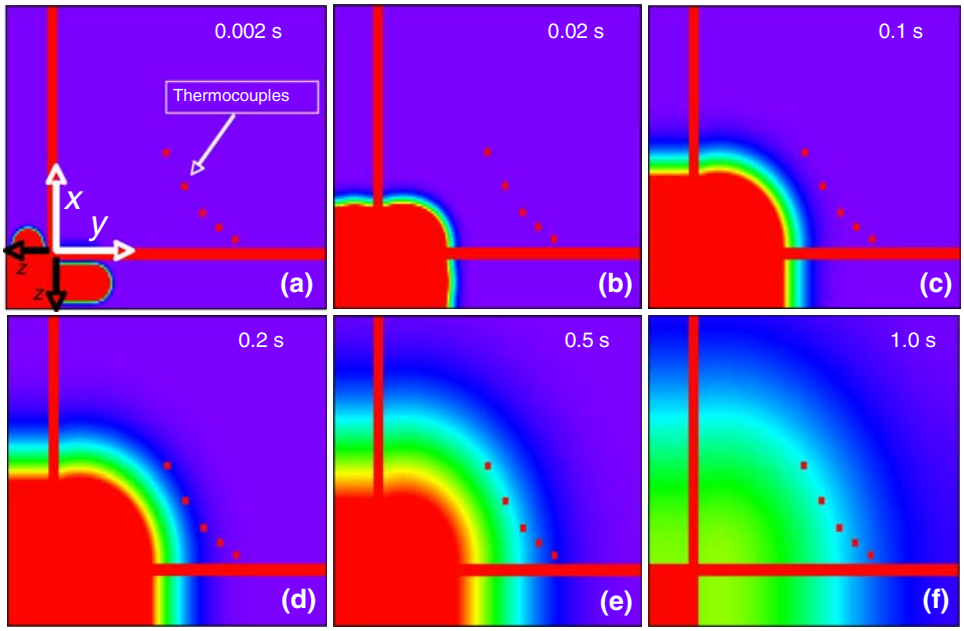

Fig. 16 Time evolution of solid-liquid interface during current pulse where line source distribution is assumed

include a characterization of the response of the material to a specified current pulse. Accordingly, the set of parameters τ_1, Δt, κ, and $C(x_k,y_k,z_k)$, $k = 1,\ldots,N_k$, can be adopted for model representation of the multiscale response of a material to localized heating by a specified current pulse.

9.1 Added Note on Observed Time Delay in Pulsed Current Contact Experiments

In actuality, the primary contribution to time delay shown in Fig. 15 is due to a manual triggering of the data acquisition system and has no physical significance. The current pulse was triggered at the spike in the temperature curve located near 2 s. About 250 ms beyond this spike the thermocouple amplifier settles and valid data are acquired. With respect to our analysis framework, however, the time shift parameter τ_1, which characterizes phenomenologically the evolution of the solidification boundary, includes the effect of any time delay associated with the initiation of energy deposition within the system.

10. Discussion

A procedure has been developed and applied that represents a general framework for the calculation of multiscale thermal diffusivities and associated process parameters. This general framework is structured for heat source field reconstruction and parameter optimization with respect to temperature field values in regions that are close to and relatively far from the energy source. The parameterizations are multiscale with respect to both multiple temperature ranges and different characteristic timescales for heat transfer.

The results of the analysis demonstrated that from a relatively small number of measured temperature histories it is possible to reconstruct consistent temperature field histories associated with an asymmetric heat source, which is induced by a high pulse current, for a domain involving a hollow cylinder. The heat source was scaled to follow the actual current in a manner that accounts for ohmic heating. The solution domain was mapped into a flat plate. This mapping was achieved via two successive symmetry cuts and unfoldings, while a third symmetry plane was used to reduce the size of the computational resources required.

An important result of this analysis is that the spatial evolution of temperature waves generated by the heat source suggests that an alternate choice of thermocouple locations may be more advantageous for analysis. In fact, this analysis provides enough information for determining a better thermocouple distribution pattern in a manner such that the sensors are not activated by the heat wavefronts essentially simultaneously (as the current configuration indicates) but rather at separate moments. This can be achieved with a thermocouple distribution that is perpendicular to the heat wavefronts.

The system parameterization presented here is that of the localized response of a metal-metal contact to an intense current pulse. This model representation provides the basis for two forms of extension for further analysis. First, this model can be embedded into coarser scale system analyses such as boundary conditions on finite element representations. And second, this model can be adopted as a global constraint on more localized and short-time scale analyses. Such analyses would adopt more detailed physical representations of the energy source. This would require, in particular, inclusion of equations representing electric current conduction and mechanical loading to account for inhomogeneity of current flow and metal-metal contact resistance, respectively.

Acknowledgments

The authors acknowledge the support by the National Science Foundation under grants EIA-0205663 and CNS-0540419. The Office of Naval Research is also greatly acknowledged for its support. Partial support from NRL's 6.1 core funding is also greatly acknowledged. We would also like to thank Mr. Scott Lord and

Prof. Andrew Smith of the U.S. Naval Academy, as well as Dr. R. Meger and Mr. Ryan Hoffman of NRL's Plasma Physics Division for their support.

References

1. H.N. Jones, J.M. Neri, C.N. Boyer, K.P. Cooper, and R.A. Meger, Pulsed Current Static Electrical Contact Experiment, *IEEE Trans. Magn.*, 2007, **43**(1), p 343
2. J. Michopoulos and S. Lambrakos, On the Fundamental Tautology of Validating Data-Driven Models and Simulations, *Int. Conf. Comput. Sci.*, 2005, **2**, p 738–745
3. J.G. Michopoulos and S.G. Lambrakos, Underling Issues Associated with Validation and Verification of Dynamic Data Driven Simulation, *Proceedings of the 2006 Winter Simulation Conference, December 3–6, 2006*, Monterey, CA, L.F. Perrone, F.P. Wieland, J. Liu, B.G. Lawson, D.M. Nicol, and R.M. Fujimoto, Eds., CD-ROM, ISBN 1-4244-0501-7, IEEE Catalog Nu. 06CH37826
4. A. Kirsch, *An Introduction to the Mathematical Theory of Inverse Problems*. Springer Verlag, New York, 1996
5. S.G. Lambrakos and J.O. Milewski, Analysis of Processes Involving Heat Deposition Using Constrained Optimization, *Sci. Technol. Weld. Join.*, 2002, **7**(3), p 137
6. J. Xie and J. Zou, Numerical Reconstruction of Heat Fluxes, *SIAM J. Numer. Anal.*, 2005, **43**(4), p 1504–1535
7. T.F. Chan and X.-C. Tai, Level Set and Total Variation Regularization for Elliptic Inverse Problems with Discontinuous Coefficients, *J. Comput. Phys.*, 2003, **193**, p 40–66
8. T.F. Chan and X.-C. Tai, Identification of Discontinuous Coefficients in Elliptic Problems Using Total Variation Regularization, *SIAM J. Sci. Comput.*, 2003, **25**, p 881–904
9. Z. Chen and J. Zou, An augmented Lagrangian Method for Identifying Discontinuous Parameters in Elliptic Systems, *SIAM J. Control Optim.*, 1999, **37**, p 892–910
10. M. Yamamoto and J. Zou, Simultaneous Reconstruction of the Initial Temperature and Heat Radiative Coefficient, *Inverse Probl.*, 2001, **17**, p 1181–1202